

A HYBRID APPROACH TO TANDEM CYLINDER NOISE

David P. Lockard*

NASA Langley Research Center, Hampton, VA 23681-2199, U.S.A.

ABSTRACT

Aeolian tone generation from tandem cylinders is predicted using a hybrid approach. A standard computational fluid dynamics (CFD) code is used to compute the unsteady flow around the cylinders, and the acoustics are calculated using the acoustic analogy. The CFD code is nominally second order in space and time and includes several turbulence models, but the SST $k - \omega$ model is used for most of the calculations. Significant variation is observed between laminar and turbulent cases, and with changes in the turbulence model. A two-dimensional implementation of the Ffowcs Williams-Hawkings (FW-H) equation is used to predict the far-field noise.

INTRODUCTION

The process of generating a structured mesh for realistic configurations with the smoothness required for high-accuracy schemes is a time-consuming and difficult process. Furthermore, high-order schemes often lack the robustness of standard low-order computational fluid dynamics (CFD) codes. Although higher-order methods have the potential to produce improved solutions in less time, the advantages are difficult to realize for certain classes of problems, such as cylinder shedding.

To resolve the shedding from tandem cylinders with a structured grid requires a multiblock capability. In addition, the grid must be highly clustered in the vicinity of the cylinders to resolve the boundary layers and separated regions. The small grid spacing places stringent requirements on the time step unless an implicit time-stepping algorithm is employed. Furthermore, the flow is typically turbulent requiring some sort of model. These capabilities are typically available in standard CFD codes, although their accuracy can be questionable for fully unsteady flows. However, if the grid and time step are chosen appropriately, good near field solutions can be obtained. The accuracy of the turbulence model for unsteady flows is an area of research, but standard models appear to perform reasonably for low-frequency phenomena such as cylinder shedding. In addition, unsteady turbulence modeling is an important issue for all algorithms, regardless of their accuracy.

The present work attempts to resolve the near field around tandem cylinders using a standard CFD code. The computations are strictly two-dimensional. The Mach and Reynolds numbers are 0.714 and 15,800, respectively, and the cylinder diameter is 0.955cm. Computing the solution all the way to far-field observers would be prohibitively expensive, so an acoustic analogy is used to predict the far-field noise. Unsteady CFD data on surfaces around the cylinders is used as input into a two-dimensional implementation of the Ffowcs Williams-Hawkings equation to determine the noise at desired observer locations. In the next section, the numerical methods are discussed. The results, timing information, and some conclusions are presented subsequently.

NUMERICAL METHOD

CFD Code

The CFD calculation employs the code CFL3D,^{1,2} developed at NASA Langley Research Center to solve the three-dimensional, time-dependent, thin-layer Reynolds-Averaged Navier-Stokes (RANS) equations. The code employs third-order differencing of the convective terms, and is second-order for the viscous terms. The finite-volume formulation employs Roe's flux difference splitting to determine the flux at cell interfaces. For time accurate cases, a dual time strategy is employed. A second-order backward difference is used to discretize the temporal derivatives. A pseudo-time term is then added to allow the steady-state machinery to be employed to converge to the solution at the next time step. Local time-stepping and multigrid are used to accelerate the convergence. Twenty-five subiterations are used to converge each time step. For the current problem, test cases were run with ten to fifty subiterations, and the solutions were nearly identical for twenty-five subiterations and above.

* Aerospace Technologist

CFL3D has a large suite of turbulence models, but only three are investigated in this work. In addition, the code was run in a fully laminar mode. Cases employing the Spalart-Allmaras³ turbulence model eventually suppressed all unsteadiness if the code was run long enough. The SST k- ω model⁴ of Menter is much less dissipative and is used for most of the runs. An Explicit Algebraic Stress (EASM) Model of Gatski⁵ is also utilized to examine the effect of a higher-order closure model. When a turbulence model was used, the entire flowfield was assumed to be turbulent. No attempt was made to simulate transition.

FW-H Solver

The Ffowcs Williams and Hawkings⁶ (FW-H) equation is an exact rearrangement of the continuity and Navier-Stokes equations. The time histories of all the flow variables are needed, but no spatial derivatives are explicitly required. The solution to the FW-H equation requires a surface and a volume integral, but the solution is often well approximated by the surface integral alone. The FW-H method has typically been applied by having the integration surface coincide with the surfaces of solid bodies, but the method is still applicable when the surface is off the body and permeable. Lockard⁷ developed an efficient, two-dimensional formulation given by

$$\begin{aligned}
 H(f)c_o^2\rho'(\mathbf{y}, \omega) = & - \oint_{f=0} F_i(\boldsymbol{\xi}, \omega) \frac{\partial G(\mathbf{y}; \boldsymbol{\xi})}{\partial \xi_i} dl - \oint_{f=0} i\omega Q(\boldsymbol{\xi}, \omega) G(\mathbf{y}; \boldsymbol{\xi}) dl \\
 & - \int_{f>0} T_{ij}(\boldsymbol{\xi}, \omega) H(f) \frac{\partial^2 G(\mathbf{y}; \boldsymbol{\xi})}{\partial \xi_i \partial \xi_j} d\boldsymbol{\xi}. \quad (1)
 \end{aligned}$$

where

$$\begin{aligned}
 F_i &= \left(p\delta_{ij} + \rho(u_i - U_i)(u_j + U_j) + \rho_o U_i U_j \right) \frac{\partial f}{\partial y_j} \text{ and} \\
 Q &= \left(\rho(u_i + U_i) - \rho_o U_i \right) \frac{\partial f}{\partial y_i}. \quad (2)
 \end{aligned}$$

The contribution of the Lighthill stress tensor, T_{ij} , is known as the quadrupole term. The dipole term F_i involves an unsteady force, and Q gives rise to a monopole-type contribution that can be thought of as an unsteady mass addition. The function $f = 0$ defines the surface outside of which the solution is desired. The total density and pressure are given by ρ and p , respectively. The fluid velocities are u_i , while the v_i represent the velocities of the surface f . The Kronecker delta, δ_{ij} , is unity for $i = j$ and zero otherwise. A prime is used to denote a perturbation quantity relative to the free-stream conditions denoted by the subscript o . The Cartesian coordinates and time are x_i and t , respectively. The usual convention involves a quiescent ambient state with f prescribed as a function of time so that it always surrounds a moving source region of interest. $H(f)$ is the Heaviside function which is unity for $f > 0$ and zero for $f < 0$. The derivative of the Heaviside function $H'(f) = \delta(f)$ is the Dirac delta function, which is zero for $f \neq 0$, but yields a finite value when integrated over a region including $f = 0$. Although the equation is written in Cartesian tensor notation, by interpreting the indices to run only over 1 and 2 it can be thought of as being in two dimensions.

RESULTS

The baseline grid for the CFD computations contains 206479 grid points in 15 blocks. Figure 1(a) shows the grid with the block boundaries in light grey. All of the block interfaces are one-to-one. The cylinder diameter $D=0.955\text{cm}$. The normal spacing on the cylinder walls is $4.4\text{e-}4$ cylinder diameters. The normal grid spacing was varied until there were minimal changes in the solution. The amplitude of the oscillations is strongly dependent on the grid spacing near the walls, but the shedding frequency is relatively insensitive.

Superimposed on the grid as white lines in Figure 1 are the surfaces used to sample data from the CFD computation for use in the FWH solver. Unsteady data was recorded on the cylinder surfaces, and on two nearly rectangular boxes around the cylinders. The penetrable surfaces are referred to as the inner and far porous surfaces.

Figure 1(b) shows the directivity results from a grid refinement study between the baseline grid and one refined by a factor of two in all directions. The pressure in the figure is nondimensionalized by $\rho_\infty c_\infty^2$. The observers are located 100 diameters from a point between the two cylinders. Although there is some variation between the results, the patterns

are similar and the peak noise radiation is nearly identical. The Strouhal number of the shedding changed from 0.222 to 0.224 between the baseline and fine grids. A detailed analysis of the fine grid results shows most differences are a result of resolving additional instabilities in the shear layers formed between the cylinders and the shedding vortices. These instabilities are somewhat artificial because of the two-dimensional nature of the calculations. In fully three-dimensional simulations, the variation in the spanwise direction tends to significantly reduce the shear layer instabilities. Therefore, all subsequent cases utilize the baseline grid.

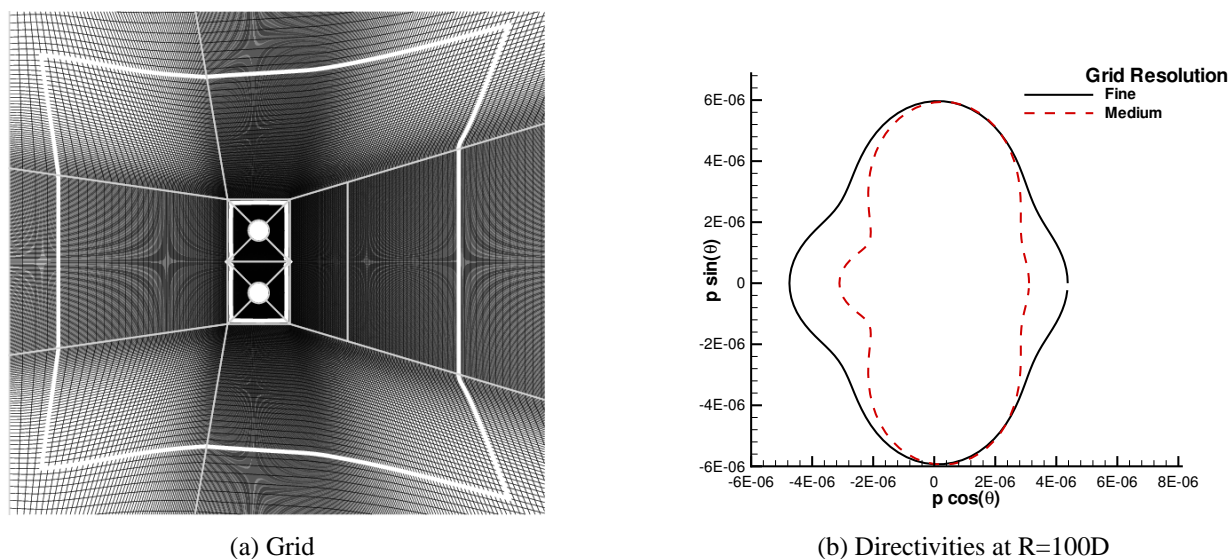


Figure 1: Baseline grid with block interfaces in grey and FWH surfaces in white and directivity comparison for grid refinement.

The near field pressure and vorticity fields for the $k-\omega$ turbulence model and laminar flow cases are shown in Figures 2 and 3. The vortex streets behind the cylinders is evident. The resolution within a few diameters of the cylinders is sufficient to maintain the vortices, but the grid coarsens significantly downstream smearing and dissipating the vortices. A comparison of the turbulent and laminar cases reveals considerably more randomness and scales for the laminar flow. The laminar results are highly grid dependent and are not believed to be indicative of the real flow. Because the grid resolution is very high in the vicinity of the cylinders, instabilities grow rapidly for this two-dimensional flow and overwhelm the solution. As the grid is refined, smaller scale instabilities develop. With a turbulence model, there is additional dissipation which suppresses most of these instabilities and synchronized shedding from the cylinders is observed. The lift and drag coefficients on the lower cylinder as a function of time for the laminar and turbulent cases are presented in Figure 4. Although there are some similarities, there is more randomness for the laminar case. A longer time record reveals much more irregularity. From the lift and drag curves, one would expect a dipole-type directivity for the resulting noise. Figure 5(a) does show considerably more noise normal to the flow direction for the laminar flow case, but the turbulent cases predict significant noise radiation in the upstream and downstream directions. Presumably, the synchronized shedding from the tandem cylinders in the turbulent cases causes the potential field to oscillate in a regular fashion resulting in the time-varying pressure fields in the streamwise direction. Both the EASM and SST $k-\omega$ turbulence models predict synchronized shedding, although the amplitude of the noise radiation is somewhat different. Table 1 gives the Strouhal numbers of the shedding for the different turbulence models.

Table 1: Strouhal numbers for different turbulence models.

Model	Strouhal Number
Laminar	0.206
EASM	0.249
SST $k-\omega$	0.222

Three time steps were used to run calculations with the SST $k-\omega$ turbulence model to investigate the effect of time resolution. Twenty-five pseudo-time subiterations were run per time step to insure convergence at each time step. Figure 5(b) shows that the results for the two smaller time steps are nearly identical, and only a small variation is observed with the largest time step. The Strouhal number varied from 0.220 to 0.223 as the time step was decreased. The time step is nondimensionalized by c_∞/D . All of the results presented in this paper were run with the smallest time step except for the grid refinement which was run with the intermediate value.

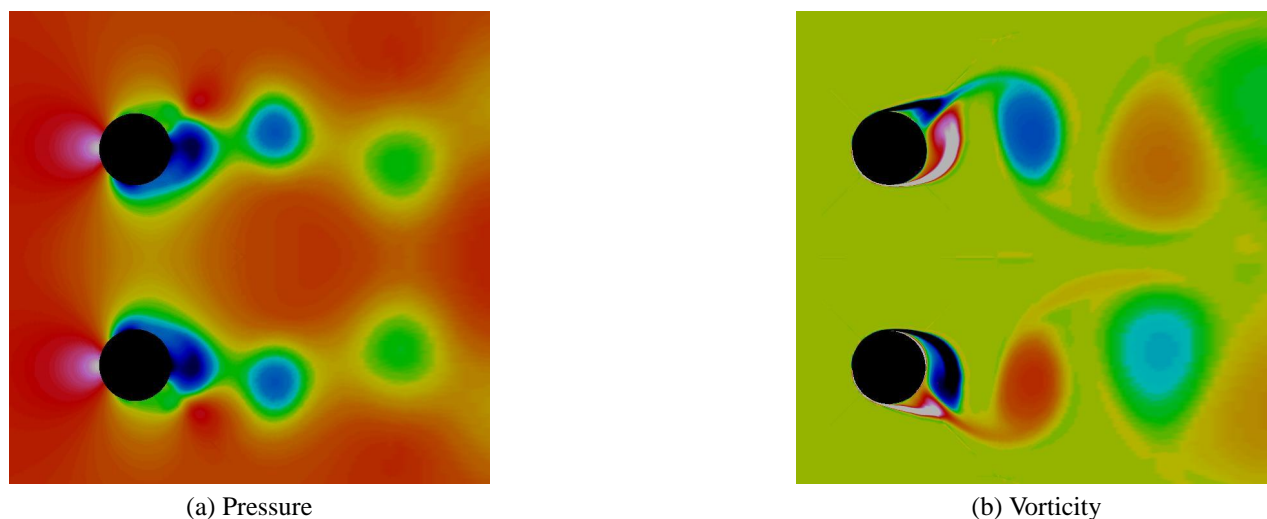


Figure 2: Instantaneous results for the SST $k-\omega$ turbulence model.

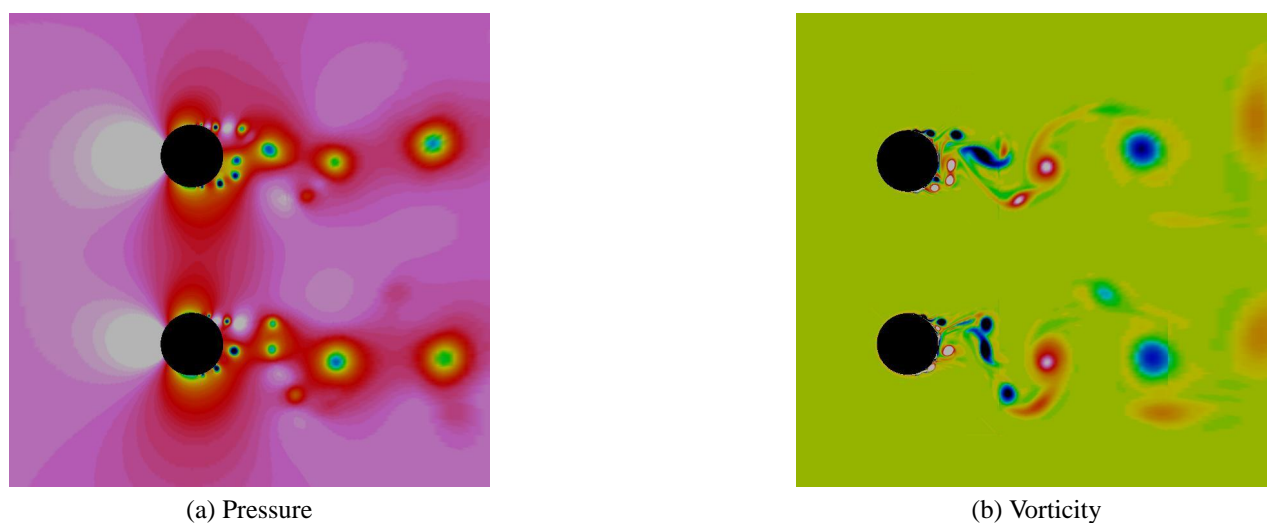


Figure 3: Instantaneous results for laminar flow.

The influence of the location of the Ffowcs Williams-Hawkins surface is examined in Figure 6. The results for observers at a radius of ten are shown in Figure 6(a), and for a radius of 100 in Figure 6(b). The observer location must be outside of the surface, but the far porous surface is beyond $R=10$, so no results are presented for the outer surface in Figure 6(a). The pressure fluctuation levels in the streamwise direction are considerably higher at $R=10$ compared with $R=100$ indicating that it is primarily a near field effect. The dominant noise radiation is normal to the flow at $R=100$, although there is still significant noise radiation upstream. For both observer distances, the agreement for different FWH surfaces is reasonable, and it is quite good for $R=100$.

The FWH equation only requires the pressure for impenetrable surfaces, but all the flow variables are needed otherwise. The advantage of a penetrable surface is that all quadrupole effects within the surface are included. Quadrupole

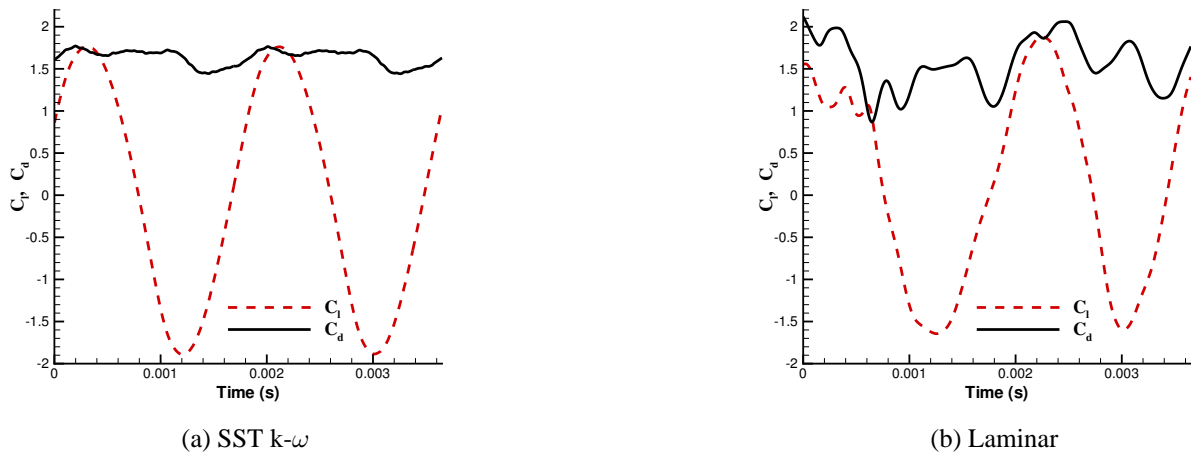


Figure 4: c_l and c_d results.

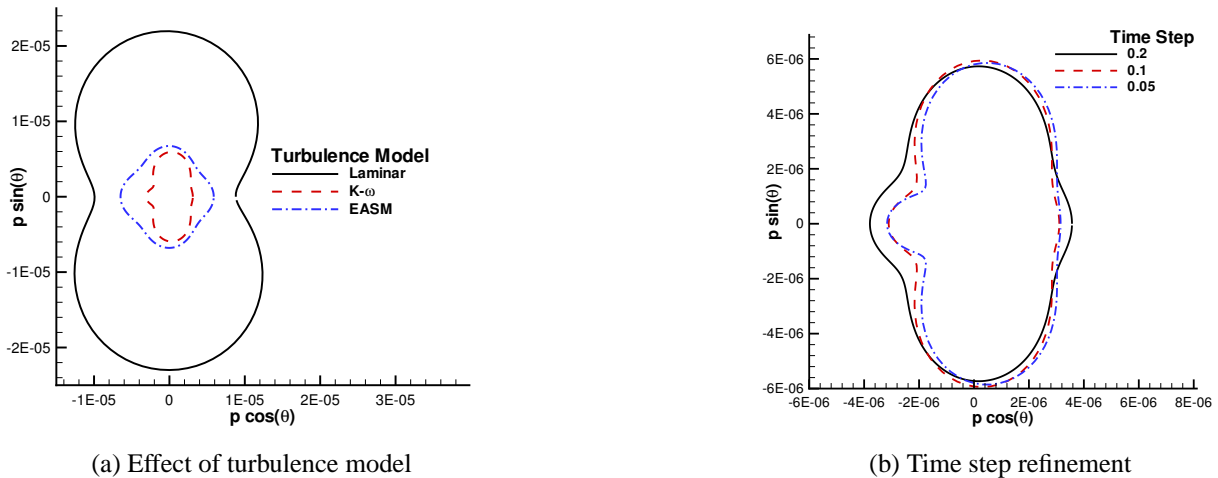


Figure 5: Time step study and influence of turbulence model for an observer at $R=100$

effects include nonlinear propagation, reflection, and refraction. For cylinder shedding, the noise tends to be at low frequencies where reflection and refraction by shear layers and unsteady flow structures tends to be minimal. Therefore, the results with the penetrable and impenetrable surfaces are not expected to differ significantly as Figure 6 demonstrates. An additional source of error for penetrable surfaces occurs when wakes pass through and generate erroneous noise because the volume integral for the quadrupole is not included. When a vortex is partially within the surface, the contribution from the surface terms should be canceled by the volume integration. However, the errors are typically much smaller than the real noise emanating from the cylinders. Another potential source of errors with penetrable surfaces is the accuracy of the input data. When the surface is far from the noise generation region, any errors in the propagation of the acoustic signal and flowfield by the CFD code will result in errors in the FWH computation. For the current problem, the wavelength is so long that it is unlikely that propagation errors are significant.

RESOURCES

A Beowulf cluster of 2.53 GHz Intel Pentium IV computers was used to run the CFD calculations. Total memory usage was approximately 500 MB for the baseline grid of 206479 points. Turbulent cases were run approximately 300 CPU hours to wash out all transients and obtain a nearly periodic state. Sampling was performed at a cost of 30 CPU hours/period. The laminar case was run considerably longer because of the randomness in the shedding. The FWH

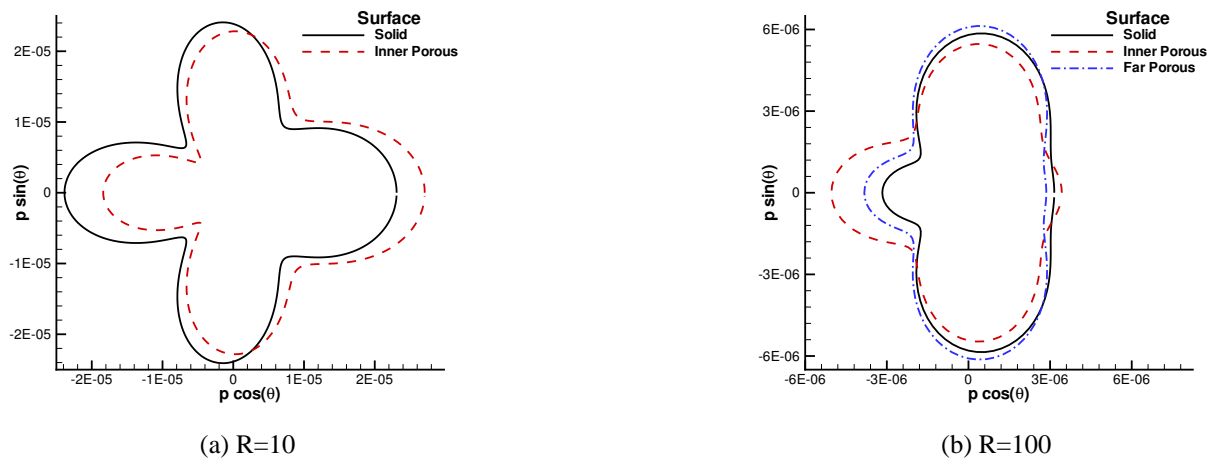


Figure 6: Directivities for $k-\omega$ turbulence model.

solver required only a few minutes to calculate the noise at 360 observer locations.

CONCLUSIONS

The hybrid coupling of a low-order CFD code with a FWH solver appears to be well suited to predicting the noise from tandem cylinders. The multiblock capability of the CFD code allowed a grid to be generated with minimal difficulty, and the robustness of the code permitted the solutions to be computed without any special treatment. The greatest source of error appears to be in the turbulence model. Although standard turbulence models perform reasonably well for low-frequency phenomena, the choice of turbulence model clearly affected the solution. Furthermore, the low Reynolds number of the the current case probably results in a transitional flow around the cylinder which was not taken into account in the current calculations.

REFERENCES

- [1] Rumsey, C.; Biedron, R.; and Thomas, J.: CFL3D: Its History and Some Recent Applications. NASA TM 1997-112861, May 1997. Presented at the Godonov's Method for Gas Dynamics Symposium, Ann Arbor, MI.
- [2] Krist, S. L.; Biedron, R. T.; and Rumsey, C.: *CFL3D User's Manual (Version 5)*. NASA Langley Research Center, Aerodynamic and Acoustic Methods Branch, 1997.
- [3] Spalart, P.; and Allmaras, S.: A One-Equation Turbulence Model for Aerodynamic Flows. *La Recherche Aeronautique*, vol. 1, no. 1, 1994, pp. 5–21.
- [4] Menter, F.; and Rumsey, C.: Assessment of Two-Equation Turbulence Models for Transonic Flows. AIAA-94-2343, 1994.
- [5] Rumsey, C.; and Gatski, T.: Summary of EASM Turbulence Models in CFL3D With Validation Test Cases. NASA TM 2003-212431, June 2003.
- [6] Ffowcs Williams, J. E.; and Hawkings, D. L.: Sound generation by turbulence and surfaces in arbitrary motion. *Philosophical Transactions of the Royal Society of London A*, vol. 342, 1969, pp. 264–321.
- [7] Lockard, D. P.: An Efficient, Two-Dimensional Implementation of the Ffowcs Williams and Hawkings Equation. *Journal of Sound and Vibration*, vol. 229, no. 4, 2000, pp. 897–911.